Hydrothermal synthesis of graphene wrapped Fe-doped TiO_2 nanospheres with high photocatalysis performance

Jiangbo Shi[a], Guiqiu Chen[a], Guangming Zeng[a*], Anwei Chen[b*], Kai He[a], Zhenzhen Huang[a], Liang Hu[a], Jingwen Zeng[a], Jing Wu[a], Weiwei Liu[a].

a. *College of Environmental Science and Engineering, Hunan University and Key Laboratory of Environmental Biology and Pollution Control (Hunan University), Ministry of Education, Changsha 410082, P.R. China*

b. *College of Resources and Environment, Hunan Agricultural University, Changsha 410128,PR China*

Corresponding authors E-mail addresses: zgming@hnu.edu.cn (G. Zeng), A.Chen@hunau.edu.cn (A. Chen). Tel.: +86 731 88822829; fax: +86 731 88823701.

Abstract

In this study, graphene wrapped Fe-doped TiO_2 (G-TiO_2-Fe) spheres were prepared through a simple hydrothermal process. The structural, optical and photocatalytic properties of synthesized composite were characterized by field emission scanning electron microscope (FE-SEM), X-ray diffraction **(**XRD), Raman Microprobe (Raman), X-ray photoelectron spectroscopy (XPS) and UV-Vis diffuse reflectance spectrophotometer (DRS). The G-TiO_2-Fe composite showed a significant red-shift in light response edge as compared with TiO_2. Meanwhile, the band gap exhibited an obvious decline from 3.24 to 2.99 eV. The photocatalytic capacity of G-TiO_2-Fe was further evaluated by methylene blue (MB) degradation experiments, and the results indicated that the optimized G-TiO_2-Fe exhibited a remarkable increase in photocatalytic activity. The superior photocatalytic performance of the novel material could be ascribed to the synthetic effects of doped Fe and wrapped graphene shells. The unique geometrical configuration and constructive component which modified the TiO_2 electronic structure will largely improve the electron transporting efficiency and restrain the electron-hole recombination.

Key words: TiO_2; Graphene; Fe doping; Photocatalysis; Methylene blue

1. Introduction

Photocatalysts, capable of utilizing solar energy for pollutant degradation and hydrogen production, have been studied to alleviate environmental deterioration and energy crisis [1-3]. Among various photocatalysts, titanium dioxide (TiO_2) is considered as one of the most suitable candidates because of its high chemical inertness, long-term stability, slight toxicity, strong oxidation and low cost [4-7]. However, with a wide band gap reached to 3.2 eV [8], TiO_2 photocatalyst only responses to ultraviolet light with a wavelength below 387 nm, which occupies about 4% of total solar spectrum. [9-11]. Thus, the photocatalytic performance of TiO_2 in wastewater treatment under solar light is restricted. In order to break the limit, many improving methods have been explored including surface modification, element doping and heterogeneous composition [12-15]. Doping has been regarded as a feasible method to modify the electronic structure of TiO_2, owing to its ability to narrow the band gap and broaden the solar absorption range. To date, it has been reported that non-metal such as C [16], B [17] and N [18], transition metal including Fe [19], Pt [20], Au [21] and Sn [22] had been successfully doped into TiO_2, and the light response wavelength of the resulting materials showed significant red-shift. Though doped with various kinds of elements increasing the light response wavelength and improving the photocatalytic performance of TiO_2, their drawbacks still exist. For example, the non-metal ions doped in TiO_2 crystal lattices are easy to be destroyed under high temperature, and some metals are quite precious, which would restrict their practical application [23]. In comparison, Fe is an abundant metal resource in nature, and it is rather stable under many complex conditions [24]. Importantly, it is easy to be doped into TiO_2 crystal lattice due to the approximate size with Ti atoms [25]. Overall, it is an excellent candidate for TiO_2 doping. Khan and

Swati [26] doped Fe^{3+} into TiO_2 nanoparticles, which resulted in a significantly enhanced photocatalytic activity for 4-chlorophenol degradation under both UV and visible irradiation. Wang et al. [23] prepared Fe doped TiO_2 nanotube arrays with enhanced photoelectrochemical performance for methylene blue (MB) degradation. Zhu et al. [27] successfully synthesized Fe doped nanocrystalline TiO_2 via a nonhydrolytic sol-gel route, which showed mesoporous structure and exhibited increased photocatalytic activity on MB degradation under visible irradiation. However, previous studies mainly focus on the individual effects of doping on the photocatalytic performance of TiO_2, and the studies referring joint effects with other nanomaterials are rare.

Graphene, a two-dimensional carbon allotrope with strict honeycomb structure, has attracted tremendous attention among academic circles since its first discovery in 2004 [28-30]. Owing to its unique structure, graphene possesses many exceptional physical and chemical characteristics, such as large surface area, efficient electric charge transfer, optical transparency as well as mechanical strength [31-34]. Therefore, it has been widely applied in many fields including pollutant adsorption, solar cell photo-electrode, photocatalysis, etc [35-40]. Notably, graphene combined with photocatalysts exhibits multiple magnificent properties. Its superior electrical conductivity, which largely separate the electron and electro-hole generated during photoelectron excitation and inhibit their rapid recombination, will contribute to the photocatalytic reaction in a large degree [41]. Furthermore, the carbon atoms arranged in the honeycomb network through an ideal sp^2 hybridization endow graphene great adsorption capacity via π-π interaction, which will facilitate the movement of organic pollutants onto the photocatalysis interface and conduce to the photochemical reaction [42-46]. With such magnificent characters, graphene has become a hot spot in

photocatalysis field, and many researches have been carried out in designing new graphene-TiO_2 hybrid materials. Zhu et al. [47] fabricated one-dimensional mesostructure TiO_2-graphene composite with enhanced photovoltaic and photocatalytic properties in dye-sensitized solar cells and photodegradation of methyl orange. Pan et al. [48] grafted TiO_2 nanowires and TiO_2 nanoparticles onto graphene sheets respectively and further identified their improved photocatalytic performance over TiO_2 towards MB under solar light. Kim et al. [49] successfully fabricated nanosized graphene coated TiO_2 nanoparticles for enhanced H_2 production and photocurrent generation rate in comparison to TiO_2 nanoparticles loading on larger graphene sheet. Based on the previous studies, we constructed a striking core/shell geometric model and wrapped thin graphene layers on the Fe-doped TiO_2 spheres to gain Fe^{3+}-doped TiO_2 core and graphene shell nanospheres. The unique structure makes TiO_2 a higher contact ratio with graphene in comparison to some other geometry like loading configuration, and that would render TiO_2 a tight integration with graphene which would hardly be detached even in some extreme condition. [49, 50] Moreover, the higher contact ratio endues TiO_2 higher electron and hole separation efficiency.

Given the above consideration, herein, a novel graphene coated Fe-doped TiO_2 (G-TiO_2-Fe) composite with high photocatalytic performance under both visible and solar light was successfully synthesized through a hydrothermal process. The photocatalysis performance of the new material was evaluated by MB photo-degradation experiments under visible and solar light. It turned out that the G-TiO_2-Fe composite showed strong photocatalytic capacity in light irradiation, and the photodegradation efficiency was far above that of anatase TiO_2. Hence, it was a

potential photocatalytic material for further practical application in organic pollutants wastewater treatment.

2. Experiment section

2.1. Materials

Graphite powder (C, ≥99.85%) was obtained from Sinopharm Chemical Reagent Co., Ltd. (3-Aminopropyl) trimethoxysilane (APTMS, 97%), Titanium isopropoxide (TTIP, 95%) and 1-Hexadecylamine (HDA, 90%) were purchased from Aladdin Industrial Corporation (Shanghai, China). H_2O_2, $KMnO_4$, H_2SO_4, HCl, ethanol (99.7%), MB, $NaNO_3$, KCl and $FeCl_3 \cdot 6H_2O$ were obtained from Sinopharm Chemical Reagent (Beijing, China).

2.2. Method

2.2.1. Graphene oxide synthesis

Graphen oxide (GO) was prepared with a modified Hummers method [51]. Briefly, 24 mL concentrated sulfuric acid was heated to 80°C and maintained constant temperature in water bath, then 6 g graphite powder, 5 g P_2O_5 and 5 g $K_2S_2O_8$ were orderly added to get a well-dispersed mixed solution. After being stirred for 4.5 h, the graphite powder was collected with suction method, washed with enough deionized water, dried under vacuum condition and grounded into powder for later use. 120 mL concentrated sulfuric acid was frozen to 4°C in an ice bath, then 5 g as-prepared graphite powder and 2.5 g $NaNO_3$ were dispersed to the solution under magnetic stirring to get a homogeneous dispersion, afterwards, 15 g $KMnO_4$ was slowly added and the dispersion was kept stirring at 4°C for 4 h. After the stage, the solution was slowly heated to 35°C, stayed stirring for another 2 h. Then the solid-liquid mixture was transferred to 240 mL pre-prepared cold deionized water, and placed in a 90°C water bath for 20 min. After the water bath heating, 720 mL deionized water was

added to stop the reaction, then 20 mL 30% hydrogen peroxide was added to remove the residual MnO_4^-, meanwhile, the solution would turn purple green into golden yellow. The solution was kept at room temperature for 2 days, and the precipitation was recovered by centrifugation and thoroughly washed with HCl (5%) and deionized water orderly. Then the well washed GO suspension was freeze-dried and re-suspended into moderate amount of deionized water to gain a required concentration of graphene oxide suspension.

2.2.2. Preparation of TiO_2 precursor with different Fe^{3+} doping amounts (TiO_2-Fe).

2.648 g HDA was dissolved in 400 mL ethanol, and then 1.6 mL 0.1 M KCl was added to obtain an uniform dispersion. Afterwards, certain amounts of $FeCl_3 \cdot 6H_2O$ (0, 5, 10 and 20 mg) were dissolved into the solution, and then 8.8 mL TTIP was added under vigorous agitating at room temperature. The resulting TiO_2 suspensions with different colors due to the different doping amounts were kept static at ambient temperature for 18 h. Ultimately, the precipitate was collected by an air pump filtering process, washed with large amount of ethanol and dried at room temperature.

2.2.3. Hydrothermal preparation of graphene wrapped Fe^{3+}-doped TiO_2 spheres (G-TiO_2-Fe).

0.4 g as-prepared TiO_2-Fe precursor was dispersed in 200 mL ethanol by ultrasonication for 30 min, then 2 mL APTMS was added into the solution. To obtain pure positive-charged TiO_2-Fe, the mixture was heated and refluxed for 4 h, washed with ethanol to remove the redundant APTMS, and filtered with a vacuum filter and dried at ambient condition. In order to wrap graphene oxide onto Fe^{3+}-doped TiO_2 spheres, 0.4 g positive-charged TiO_2-Fe was suspended into pre-prepared negative charged GO suspension, and then the resulting mixture was sonicated for 20 min. The

composite (GO-amorphous TiO_2-Fe) was recovered through filtration and transferred into a 50 mL Teflon-lined stainless steel vessel using 20 mL ethanol and 10 mL deionized water as solvent. Then reactors were placed in oven at 180°C for 16 h. Ultimately, the material was calculated at 400°C in argon atmosphere for 2 h. The final hydrothermal-treated materials prepared with 0, 5, 10 and 20 mg $FeCl_3 \cdot 6H_2O$ were defined as G-TiO_2-Fe (0), G-TiO_2-Fe (5), G-TiO_2-Fe (10) and G-TiO_2-Fe (20), respectively.

2.3. Photocatalytic activity test

Photo-degradation reactions were conducted with an autonomous photo reactor. The solar light was simulated by a 300 W xenon (Xe) lamp purchased from CeAulight China. A 420 nm light filter was used to gain visible light. 100 mL MB with a concentration of 10 mg/L was poured in a glass container, and then 50 mg material was added into the vessel. In order to reach adsorption/desorption equilibration, the mixed solution was agitated for an hour in dark condition [52]. Next, the reaction vessel was transferred to the visible (solar) light environment and kept stirring for another 2 h (1 h). During the photoreaction stage, 3 mL suspension was sampled every 15 min (10 min). After being centrifuged, the sample concentration was measured with ultraviolet spectrophotometry.

2.4. Characterization

Field emission scanning electron microscope (FE-SEM, MIRA 3 LMU/X-Max20/H1002) equipped with an energy dispersive spectrometer (EDS, INCA 250) was used to investigate the morphology and the components of G-TiO_2-Fe. X-ray diffraction (XRD, SIMENS D500) with Cu-Ka radiation (λ=1.54184 Å) was applied to analyze phase change of the materials after hydrothermal reaction. X-ray photoelectron spectroscopy (XPS, K-Alpha 1063) purchased from Thermo Fisher was

used to quantify the valence state and composition of G-TiO_2-Fe. UV-Vis diffuse reflectance spectrophotometer (U3900, Hitachi) was used to measure the optical adsorption discrepancy of composite materials with different Fe^{3+} doping amount. UV-vis spectrophotometer (UV-2550) was used to measure the MB concentration during the photo-degradation process. Raman Microprobe (Labram-010) with 632 nm laser light was applied to investigate the redox state change of GO.

3. Results and discussion

3.1. Characterization of synthesized materials

According to the SEM image (Fig. 1a), the GO was successfully synthesized, and the GO nanosheet was quite thin, which would ensure its high optical transmittance. The amorphous TiO_2 was synthesized through a sol-gel process, and the samples with different $FeCl_3 \cdot 6H_2O$ adding amounts presented obvious distinctions in color (Fig. 1b). The color of TiO_2 precursor was pure white, while the TiO_2-Fe precursor changed from light yellow to orange with the increasing amount of $FeCl_3 \cdot 6H_2O$. Commonly, to be better wrapped by GO, the amorphous TiO_2 was modified with APTMS to get a positive charged surface. Zeta potential analysis was performed to detect the potential change during the wrapping process. The zeta potential of amorphous TiO_2 increased from -20.5 to 14.4 mV after being modified with APTMS, indicating that the positive changed amorphous TiO_2 was successfully obtained. To investigate the potential changes of GO after being mixed with the modified amorphous TiO_2, further zeta potential analysis was conducted. After GO suspension was mixed with the prepared positively-charged TiO_2, the surface charge of the composite increased dramatically to -6.5 mV from -40.3 mV, which indicated that GO and TiO_2 were successfully integrated through electrostatic interaction. To investigate the interior structure change, XRD and Raman spectrum were conducted.

XRD pattern was performed from 15° to 80° in 2θ with 0.02° steps/s, and the result is shown in Fig. 2. It was obvious that the as-prepared TiO_2 precursor showed no characteristic peaks which confirmed its amorphous phase. According to JCPDS card NO. 21-1272, the characteristic peaks of hydrothermal-treated TiO_2 at 2θ of 25.42°, 37.98°, 48.10°, 54.18°, 55.15°, 62.98°, 69.02°, 70.35° and 75.32° were assigned to the (101), (004), (200), (105), (211), (204), (116), (220) and (215) cyastallographic plane of anatase-phase TiO_2, respectively. The G-TiO_2-Fe presented identical peaks, except for small deviates in peak position which could be caused by the doped Fe^{3+}. As we know, the Fe^{3+} doped into the crystal lattice would cause lattice expansion and lead to left-shift of the diffraction peaks, for the subtle distinction of Fe^{3+} (0.064 nm) and Ti^{4+} (0.068 nm) in ionic radii [23]. Therefore, amorphous TiO_2 was well crystallized during the hydrothermal treatment. In addition, the diffraction peaks of G-TiO_2-Fe hybrids did not show any impurity of Fe_2O_3 or Fe_3O_4 phase, which could also validate the substitution of Fe^{3+} ions into the TiO_2 crystal lattices. It followed that the doping and wrapping treatments did not affect the TiO_2 crystallization. The Raman analysis result is presented in Fig. 3, and the peaks at 153, 399, 519 and 641 cm^{-1} corresponded to E_g, B_{1g}, A_{1g} and E_g of anatase TiO_2 phase, respectively. Peaks at 1329 and 1597 cm^{-1} were assigned to D and G band of graphene materials, respectively [53]. The intensity ratio of D and G band (I_D/I_G) is usually seen as an index to indicate the degree of defects presented in graphene materials. As is evident from the Raman spectra, the slight increase of I_D/I_G from 1.00 to 1.09 after the hydrothermal process revealed the existence of higher defects in the hybrid. It might be caused by the preceding hydrothermal treatment during which few fragmented smaller sp^2 domains formed and exfoliated from the TiO_2 surface leading to a high intensity of D band [54]. In addition, slight red-shift of G band from 1597 to 1605 cm^{-1} was observed.

Both the I_D/I_G and red-shift of G band confirmed the successful reduction of wrapped GO [13, 53]. Meanwhile, the color change of hybrid material from brown to black after the hydrothermal treatment could also reflect the reduction process.

Fig. 4 showed the FE-SEM images of amorphous TiO_2 precursor (Fig. 4a), anatase TiO_2 (Fig. 4b) and G-TiO_2-Fe (Fig. 4c). The prepared amorphous TiO_2 spheres possessed an average diameter of 1150 ± 50 nm. According to the images and the corresponding XRD analysis, it is easy to see that the amorphous TiO_2 was crystalized to form uniform spheres with a diameter of 1000 ± 50 nm after the hydrothermal treatment. The slightly reduction in sphere size could be attributed to the more regularly arranged atoms in crystal. Besides, it could be found that the crystal TiO_2 spheres consisted of many small nanocrystals and possessed relatively rough surfaces. In contrast, with graphene wrapped outside, the G-TiO_2-Fe spheres possessed very smooth surfaces and presented no obvious granular features. It could be clearly seen that the TiO_2 sphere was well coated by graphene with some winkles on its surface, which indicated the successful wrapping treatment. The EDS analysis was further performed to verify the component of G-TiO_2-Fe. As shown in Fig. 4d and Fig. 4e, the hybrids were composed of C, O, Si Ti and Fe which could also validate the successful doping of Fe. The doped Fe occupied a Fe content of 0.47% and a Fe/Ti atomic ratio of 0.16. The Si existed in the composites was originated from the ATPMS used during the TiO_2 modification procedure as well as the sample holder. Since the EDS result only revealed the ingredients and percentages of the composites, XPS was conducted to investigate the further details about the valence state and composition.

The component and valence state of the composites were determined by XPS analysis. Fig. 5 showed the XPS core level spectra of C 1s, O 1s, Ti 2p and Fe 2p in

G-TiO_2-Fe composite. The full XPS spectrum validated the main component elements of Ti, O, C and Fe, which was in reasonable agreement with the EDS results. The weak intensity of Fe spectrum was ascribed to the small doping amount. The detailed XPS results of Ti 2p region around 455-468 eV, O 1s region around 525-535 eV, C 1s region around 282-291 eV and Fe 2p region around 705-735 eV were displayed in Fig. 5 The Ti 2p core level (Fig. 5a) exhibited two major characteristic doublet at 459.43 and 465.12 eV, respectively, which was attributed to the spin orbital splitting of $2p_{3/2}$ and $2p_{1/2}$ states. The O 1s XPS spectrum (Fig. 5b) showed a strong peak at 530.14 eV, and it could be deconvoluted into three peaks at 530.01, 530.56 and 531.90 eV, which were ascribed to the surface adsorbed oxygen and hydroxyl, oxygen of TiO_2 and oxygen vacancies, respectively. After deconvolution process, the C 1s XPS spectrum (Fig. 5c) could also be resolved into three peaks: the first peak at 284.73 eV could be attributed to the C-C and C=C bonds in graphene, the second peak at 285.80 eV was ascribed to C-OH bonds existing in graphene edge, and the third peak at 286.91 eV was assigned to C=O due to the incomplete reduction. The Fe 2p core level XPS spectrum (Fig. 5d) displayed two major characteristic peaks at 710.61 and 725.33 eV for Fe $2p_{3/2}$ and Fe $2p_{1/2}$, respectively. After the further peak deconvolution it could be resolved into four peaks located at 708.73, 710.65, 714.85, 724.80 eV. The peaks at 710.65 and 724.80 eV were attributed to the doped Fe^{3+}, while the peaks at 708.73 and 714.85 eV were attributed to Fe^{2+}, which might form during the hydrothermal process for the high temperature and pressure. Thus, we could conclude that the doped Fe was major in the form of Fe^{3+} state.

The UV-vis diffuse reflectance spectra (DRS) of G-TiO_2-Fe with different Fe doping amounts are presented in Fig. 6a. The adsorption spectrum of anatase TiO_2 indicated that TiO_2 could only adsorb ultraviolet light with a wavelength below 400

nm, which was attributed to its broad band gap. In comparison, the absorption edge of G-TiO_2-Fe (0) exhibited a significant red-shift which is well coincident with previous study [1]. In addition, it is noteworthy that all of the G-TiO_2-Fe composites with Fe doped exhibit obvious red-shift in light response as compared to TiO_2. The red-shift was ascribed to the intense interaction between TiO_2 energy band and the d-electrons of the doped Fe^{3+} as well as graphene. Furthermore, the intercepts of the tangents to the $(ahv)^2$ vs. photon energy (hv) plots of each hybrid materials was obtained in virtue of Kubelka-Munk remission function. As is shown in Fig. 6b, the band gaps of TiO_2, G-TiO_2-Fe (0), G-TiO_2-Fe (5), G-TiO_2-Fe (10) and G-TiO_2-Fe (20) were estimated at 3.24, 3.04, 2.99 and 2.37 eV, respectively. The distinguished performance of utilizing visible light makes the hybrid material a superior candidate in solar cell and photo-catalysts.

3.2. Photocatalytic activity

In order to investigate the photocatalytic activity of the hybrid materials with different Fe doping amounts, the photo-degradation of MB tests were conducted under visible and solar light, respectively. As is shown in Fig. 7, the photo-degradation curves exhibited approximate trends under both irradiation conditions. MB showed little self-degradation, and the bare anatase TiO_2 exhibited relatively low catalytic capacity. In contrast, TiO_2 wrapped by graphene and doped with different amounts of Fe showed discriminating degradation efficiency. The disparities in photocatalytic performance could be attributed to the synergetic effect of graphene and Fe^{3+}. The graphene wrapped outside the spheres was beneficial to improve the electron and hole separation efficiency and gave rise to an enhanced photocatalysis capability [1], which could account for the higher photodegradation of G-TiO_2-Fe (0) compared to bare TiO_2. To our surprise, the photocatalytic activity of the hybrid

materials with different Fe doped amounts showed great distinctions. Compared to anatase TiO_2, G-TiO_2-Fe (5) and G-TiO_2-Fe (10) showed significant increase in photo degradation efficiency, whereas G-TiO_2-Fe (20) exhibited a dramatical reduction in identical situation. As we know, Fe^{3+} could make influence on the electron and hole combination process. Fe^{3+} could serve as electrons and holes trapper. The doped Fe^{3+} could be reduced to Fe^{2+} through photoelectron capture and further be re-oxidized to Fe^{3+} by the O_2 molecules existing in the mediums, thus, accomplish the electron transmission. Therefore, when a small amount of Fe^{3+} was doped, it was beneficial to the electron and hole separation and gave rise to an improved photo-degradation activity. Nevertheless, when large amount of Fe^{3+} was doped, the distance among trappers would sharply decline, and Fe^{3+} would turn into recombination centers. The trapped electron would deliver to the hole directly, which would lead to a low photocatalytic activity [55, 56].

3.3. Photocatalytic mechanism

A proposed transfer pathway for charge carriers in the G-TiO_2-Fe (10) composite is shown in Fig. 8 to clarify the enhanced photocatalytic performance. As is evident from the UV-vis DRS analysis, the G-TiO_2-Fe composite exhibits red-shifted light adsorption edge and narrowed band gap, which indicate that the doping Fe^{3+} and wrapping graphene play important roles in modifying the band structure of TiO_2 due to the d-d transition of Fe^{3+} ions and conducting band (CB) electrons, and charge transfer among CB electrons, interacting Fe^{3+} ions and graphene.

Fe^{3+} can serve as hole trapper ($Fe^{3+} + h^+ \rightarrow Fe^{4+}$) owing to the slight higher energy level than TiO_2 valence band. The trapped holes would be delivered to the surface adsorbed hydroxyl to produce hydroxyl radicals ($Fe^{4+} + OH^- \rightarrow Fe^{3+} + OH^{\bullet}$). Fe^{3+} can also act as trapping sites for photogenerated electrons to form Fe^{2+} ($Fe^{3+} + e^- \rightarrow Fe^{2+}$).

The Fe^{2+} is quite unstable and tends to re-form Fe^{3+} due to the destruction of half-filled $3d^5$ electronic configuration. The Fe^{2+} would be oxidized by the surface adsorbed O_2 molecule and produce $O_2^{-\bullet}$ ($Fe^{2+} + O_2(ads) \rightarrow Fe^{3+} + O_2^{-\bullet}$). The $O_2^{-\bullet}$ are easy to be captured by the photoinduced h^+ and produce $O^{-\bullet}$ which would be further converted to hydroxyl radicals by surface adsorbed H_2O ($O_2^{-\bullet} + h^+ \rightarrow O^{-\bullet}$; $O^{-\bullet} + H_2O(ads) \rightarrow OH^{\bullet} + OH^-$) [57]. Additionally, the work function of graphene (4.2-4.5 eV) is slightly lower than the conduction band of Fe-doped TiO_2, and the excited electrons would be delivered to the conduction band of graphene, which would lead to a narrowed band gap hindering charge recombination [58].

4. Conclusion

In summary, we successfully synthesized a graphene wrapped Fe^{3+}-doped TiO_2 composite with high photocatalytic activity through a simple hydrothermal treatment combined with sol-gel method. The G-TiO_2-Fe (10) performed higher photo-degradation efficiency toward MB in compare to TiO_2 and G-TiO_2-Fe with other doping amounts. The superior photocatalysis of G-TiO_2-Fe (10) under light irradiation could be ascribed to the synergistic effect of graphene and doped Fe^{3+}. The moderate doping Fe^{3+} acting as "electrons and holes trapper" and conducing to an efficient charge separation is beneficial to photocatalysis. Besides, the graphene wrapped outside is conductive to the electron transfer. Moreover, the graphene could also act as adsorbent and conduce to a more efficient transmission of organic compound toward photo-reaction interface through π-π interaction. Therefore, the novel G-TiO_2-Fe composite provides new insights in improving TiO_2 photocatalytic performance and shows great potential in environmental application.

Acknowledgements

This study was financially supported by the National Natural Science Foundation of China (51579099, 51521006 and 51508186), the Program for Changjiang Scholars and Innovative Research Team in University (IRT-13R17), the Hunan Provincial Natural Science Foundation of China (2016JJ3076), and the Hunan Provincial Innovation Foundation for Postgraduate (CX2016B134).

Compliance with Ethical Standards:

Conflict of Interest: The authors declare that they have no conflict of interest.

References

[1] J. S. Lee, K. H. You, C. B. Park, Highly Photoactive, Low Bandgap TiO_2 Nanoparticles Wrapped by Graphene, Adv. Mater. (2012) 1084–1088.

[2] P. Xu, G. M. Zeng, D. L. Huang, C. L. Feng, S. Hu, M. H. Zhao, C. Lai, Z. Wei, C. Huang, G. X. Xie, Z. F. Liu, Use of iron oxide nanomaterials in wastewater treatment: A review, Sci. Total Environ. 424 (2012) 1–10.

[3] M. Chen, P. Xu, G. Zeng, C. Yang, D. Huang, J. Zhang, Bioremediation of soils contaminated with polycyclic aromatic hydrocarbons, petroleum, pesticides, chlorophenols and heavy metals by composting: Applications, microbes and future research needs, Biotechnol. Adv. 33 (2015) 745–755.

[4] M. Dahl, Y. Liu, Y. Yin, Composite Titanium Dioxide Nanomaterials, Chem. Rev. 114 (2014) 9853–9889.

[5] J. Zhang, M. Vasei, Y. Sang, H. Liu, J. P. Claverie, TiO_2@Carbon Photocatalysts: The Effect of Carbon Thickness on Catalysis, ACS Appl. Mater. Interfaces. 8 (2016) 1903–1912.

[6] A. Chen, G. Zeng, G. Chen, X. Hu, M. Yan, S. Guan, C. Shang, L. Lu, Z. Zou, G. Xie, Novel thiourea-modified magnetic ion-imprinted chitosan/TiO_2 composite for simultaneous removal of cadmium and 2,4-dichlorophenol, Chem. Eng. J. 191 (2012) 85–94.

[7] M. Cheng, G. M Zeng, D. L Huang, C. Lai, P. Xu, C. Zhang, Y. Liu, Hydroxyl radicals based advanced oxidation processes (AOPs) for remediation of soils contaminated with organic compounds: A review, Chem. Eng. J. 284 (2016) 582–598.

[8] X. Zhou, N. Liu, P. Schmuki, Photocatalysis with TiO_2 Nanotubes: "Colorful" Reactivity and Designing Site-Specific Photocatalytic Centers into TiO_2 Nanotubes, Catal. 7 (2017) 3210–3235.

[9] S. Liu, H. Sun, S. Liu, S. Wang, Graphene facilitated visible light photodegradation of methylene blue over titanium dioxide photocatalysts, Chem. Eng. J. 214 (2013) 298–303.

[10] I. C. Kang, Q. Zhang, S. Yin, T. Sato, F. Saito, Improvement in photocatalytic activity of TiO_2 under visible irradiation through addition of N-TiO_2, Environ. Sci. Technol. 42 (2008) 3622–3626.

[11] S. Liu, Q. Hu, J. Qiu, F. Wang, W. Lin, F. Zhu, C. Wei, N. Zhou, G. Ouyang, Enhanced Photocatalytic Degradation of Environmental Pollutants under Visible Irradiation by a Composite Coating, Environ. Sci. Technol. 51 (2017) 5137–5145.

[12] L. Li, L. Yu, Z. Lin, G. Yang, Reduced TiO_2-Graphene Oxide Heterostructure As Broad Spectrum-Driven Efficient Water-Splitting Photocatalysts, ACS Appl. Mater. Interfaces. 8 (2016) 8536–8545.

[13] S. D. Perera, R. G. Mariano, K. Vu, N. Nour, O. Seitz, Y. Chabal, K. J. Balkus, Hydrothermal Synthesis of Graphene-TiO_2 Nanotube Composites with Enhanced Photocatalytic Activity, Catal. 2 (2012) 949–956.

[14] C. Yang, H. Chen, G. Zeng, G. Yu, S. Luo, Biomass accumulation and control strategies in gas biofiltration, Biotechnol. Adv. 28 (2010) 531–540.

[15] T. Leshuk, R. Parviz, P. Everett, H. Krishnakumar, R. A. Varin, F. Gu. Photocatalytic Activity of Hydrogenated TiO_2, ASC Appl. Mater. Interfaces. 5 (2013), 1892–1895.

[16] S. Shanmugam, A. Gabashvili, D. S. Jacob, J. C. Yu, A. Gedanken, Synthesis and Characterization of TiO_2 @C Core−Shell Composite Nanoparticles and Evaluation of Their Photocatalytic Activities, Chem. Mater. 18 (2006) 2275–2282.

[17] B. Liu, A. Khare, E. S. Aydil, TiO_2–B/Anatase Core–Shell Heterojunction Nanowires for Photocatalysis, ACS Appl. Mater. Interfaces. 3 (2011) 4444–4450.

[18] S. Q. Wang, W. B. Liu, P. Fu, W. L. Cheng, Enhanced photoactivity of N-doped TiO_2 for Cr(VI) removal: Influencing factors and mechanism, Korean J. Chem. Eng. 34 (2017) 1584–1590.

[19] R. Cai, A New Role for Fe^{3+} in TiO_2 Hydrosol□: Accelerated Photodegradation of Dyes under Visible Light, Environ. Sci. Technol. 42 (2008) 5759–5764.

[20] Z. Zhao, Theoretical Study of Pt Cocatalyst Loading on Anatase TiO_2 (101) Surface: From Surface Doping to Interface Forming, J. Phys. Chem. C. 118 (2014) 24591–24602.

[21] C. Yogi, K. Kojima, T. Hashishin, N. Wada, Y. Inada, E. Della Gaspera, M. Bersani, A. Martucci, L. Liu, T. Sham, Size Effect of Au Nanoparticles on TiO_2 Crystalline Phase of Nanocomposite Thin Films and Their Photocatalytic Properties, J. Phys. Chem. C. 115 (2011) 6554–6560.

[22] M. Xu, H. Wu, D. Zhao, G. Zheng, Controlled Sn-Doping in TiO_2 Nanowire Photoanodes with Enhanced Photoelectrochemical Conversion, Nano Lett. 2 (2012) 1503–1508.

[23] Q. Wang, R. Jin, M. Zhang, S. Gao, Solvothermal preparation of Fe-doped TiO_2 nanotube arrays for enhancement in visible light induced photoelectrochemical performance, J. Alloy. Compd. 690 (2017) 139–144.

[24] F. Long, J. L. Gong, G. M. Zeng, L. Chen, X. Y. Wang, J. H. Deng, Q. Y. Niu, H. Y. Zhang, X. R. Zhang, Removal of phosphate from aqueous solution by magnetic Fe-Zr binary oxide, Chem. Eng. J. 171 (2011) 448–455.

[25] R. D. S. Santos, G. A. Faria, C. Giles, C. A. P. Leite, H. D. S. Barbosa, M. A. Z. Arruda, C. Longo, Iron insertion and hematite segregation on Fe-doped TiO_2 nanoparticles obtained from sol-gel and hydrothermal methods, ACS Appl. Mater. Interfaces. 4 (2012) 5555–5561.

[26] H. Khan, I. K. Swati, Fe^{3+}-doped Anatase TiO_2 with d-d Transition, Oxygen Vacancies and Ti^{3+} Centers: Synthesis, Characterization, UV-vis Photocatalytic and Mechanistic Studies, Ind. Eng. Chem. Res. 55 (2016) 6619–6633.

[27] J. Zhu, J. Ren, Y. Huo, Z. Bian, H. Li, N. S. Route, Nanocrystalline Fe/TiO_2 Visible Photocatalyst with a Mesoporous Structure Prepared via a Nonhydrolytic Sol−Gel Route, J. Phys. Chem. C. 111 (2007) 18965–18969.

[28] Y. Shen, B. Chen, Sulfonated Graphene Nanosheets as a Superb Adsorbent for Various Environmental Pollutants in Water, Environ. Sci. Technol. 49 (2015) 7364–7372.

[29] Z. H. Zhang, L. D. Zhang, W. Li, A. S. Yu, P. Y. Wu, Carbon-Coated Mesoporous TiO_2 Nanocrystals Grown on Graphene for Lithium-Ion Batteries, ACS Appl. Mater. Interfaces. 7 (2015) 10395–10400.

[30] J. H. Deng, X. R. Zhang, G. M. Zeng, J. L. Gong, Q. Y. Niu, J. Liang, Simultaneous removal of Cd(II) and ionic dyes from aqueous solution using magnetic graphene oxide nanocomposite as an adsorbent, Chem. Eng. J. 226 (2013) 189–200.

[31] Y. Shen, Q. Fang, B. Chen, Environmental Applications of Three-Dimensional Graphene-Based Macrostructures□: Adsorption, Transformation, and Detection, Environ. Sci. Technol. 49 (2015) 67−84.

[32] J. L. Gong, B. Wang, G. M. Zeng, C. P. Yang, C. G. Niu, Q. Y. Niu, W. J. Zhou, Y. Liang, Removal of cationic dyes from aqueous solution using magnetic multi-wall carbon nanotube nanocomposite as adsorbent, J. Hazard. Mater. 164 (2009) 1517–1522.

[33] K. He, G. Chen, G. Zeng, M. Peng, Z. Huang, J. Shi, T. Huang, Stability, transport and ecosystem effects of graphene in water and soil environments, Nanoscale. 9 (2017) 5370–5388.

[34] H. Wu, C. Lai, G. Zeng, J. Liang, J. Chen, J. Xu, J. Dai, X. Li, J. Liu, M. Chen, L. Lu, L. Hu, J. Wan, The interactions of composting and biochar and their implications for soil amendment and pollution remediation: a review, Crit. Rev. Biotechnol. 37 (2017) 754–764.

[35] W. W. Tang, G. M. Zeng, J. L. Gong, J. Liang, P. Xu, C. Zhang, B. Bin Huang, Impact of humic/fulvic acid on the removal of heavy metals from aqueous solutions using nanomaterials: A review, Sci. Total Environ. 468-469 (2014) 1014–1027.

[36] Y. Zhang, G. M. Zeng, L. Tang, J. Chen, Y. Zhu, X. X. He, Y. He, Electrochemical sensor based on electrodeposited graphene-Au modified electrode and nanoau carrier amplified signal strategy for attomolar mercury detection, Anal. Chem. 87 (2015) 989–996.

[37] J. Wang, Z. Chen, B. Chen, Adsorption of Polycyclic Aromatic Hydrocarbons by Graphene and Graphene Oxide Nanosheets Adsorption of Polycyclic Aromatic Hydrocarbons by Graphene and Graphene Oxide Nanosheets, Environ. Sci. Technol. 48 (2014) 4817–4825.

[38] Y. Kusumawati, M. A. Martoprawiro, T. Pauporte. Effects of Graphene in Graphene/TiO_2 Composite Films Applied to Solar Cell Photoelectrode, J. Phys. Chem. C. 118 (2014) 9974–9981.

[39] Y. Cheng, H. He, C. Yang, G. Zeng, X. Li, H. Chen, G. Yu, Challenges and solutions for biofiltration of hydrophobic volatile organic compounds, Biotechnol. Adv. 34 (2016) 1091–1102.

[40] Y. H. Zhang, Z. R. Tang, X. Z. Fu, Y. J. Xu, TiO_2−Graphene Nanocomposites for Gas-Phase Photocatalytic Degradation of Volatile Aromatic Pollutant: Is TiO_2−Graphene Truly Different from Other TiO_2−Carbon Composite Materials?, Nano. 4 (2010) 7303–7314.

[41] X. Cao, Z. Yin, H. Zhang, Three-dimensional graphene materials: preparation, structures and application in supercapacitors, Energy Environ. Sci. 7 (2014) 1850–1865.

[42] J. Liang, Z. X. Yang, L. Tang, G. M. Zeng, M. Yu, X. D. Li, H. P. Wu, Y. Y. Qian, X. M. Li, Y. Luo, Changes in heavy metal mobility and availability from contaminated wetland soil remediated with combined biochar-compost, Chemosphere. 181 (2017) 281–288.

[43] J. Sun, H. Zhang, L. H. Guo, L. Zhao, Two-dimensional interface engineering of a titania-graphene nanosheet composite for improved photocatalytic activity, ACS Appl. Mater. Interfaces. 5 (2013) 13035–13041.

[44] X. F.Tan, Y. G. Liu, G. M. Zeng, X. Wang, X. J. Hu, Y. L. Gu, Z. Z. Yang, Application of biochar for the removal of pollutants from aqueous solutions, Chemosphere. 125 (2015) 70–85.

[45] C. Zhang, C. Lai, G. M. Zeng, D. L. Huang, C. P. Yang, Y. Wang, Y. Y. Zhou, M. Cheng, Efficacy of carbonaceous nanocomposites for sorbing ionizable antibiotic sulfamethazine from aqueous solution, Water Res. 95 (2016) 103–112.

[46] S. Zhuang, X. Xu, B. Feng, J. Hu, Y. Pang, G. Zhou, L. Tong, Correction to Photogenerated Carriers Transfer in Dye−Graphene−SnO_2 Composites for Highly Efficient Visible-Light Photocatalysis, ACS Appl. Mater. Interfaces. 6 (2014) 613–621.

[47] P. N. Zhu, A. S. Nair, S. J. Peng, S. Y. Yang, S. Ramakrishna, Facile fabrication of TiO_2-graphene composite with enhanced photovoltaic and photocatalytic properties by electrospinning, ACS Appl. Mater. Interfaces. 4 (2012) 581–585.

[48] X. Pan, Y. Zhao, S. Liu, C. L. Korzeniewski, S. Wang, Z. Fan, Comparing Graphene-TiO_2 Nanowire and Graphene-TiO_2 Nanoparticle Composite Photocatalysts, ACS Appl. Mater. Interfaces. 4 (2012) 3944–3950.

[49] H. I. Kim, S. Kim, J. K. Kang, W. Choi, Graphene o xide embedded into TiO_2 nanofiber: Effective hybrid photocatalyst for solar conversion, J. Catal. 309 (2014) 49–57.

[50] H. I. Kim, G. H. Moon, D. Monllor-Satoca, Y. Park, W. Choi, Solar photoconversion using graphene/TiO_2 composites: Nanographene shell on TiO_2 core versus TiO_2 nanoparticles on graphene sheet, J. Phys. Chem. C. 116 (2012) 1535–1543.

[51] W. S. Hummers, R. E. Offeman, Preparation of Graphitic Oxide, J. Am. Chem. Soc. 80 (1958) 1339–1339.

[52] P. Xu, G.M. Zeng, D. L. Huang, C. Lai, M. H. Zhao, Z. Wei, N. J. Li, C. Huang, G. X. Xie, Adsorption of Pb(II) by iron oxide nanoparticles immobilized *Phanerochaete chrysosporium*: Equilibrium, kinetic, thermodynamic and mechanisms analysis, Chem. Eng. J. 203 (2012) 423–431.

[53] S. Mukhopadhyay, D. Maiti, A. Saha, P. S. Devi, Shape Transition of TiO_2 Nanocube to Nanospindle Embedded on Reduced Graphene Oxide with Enhanced Photocatalytic Activity, Cryst. Growth Des. 16 (2016) 6922–6932.

[54] G. Lui, J. Y. Liao, A. S. Duan, Z. S. Zhang, M. Fowler, A. P. Yu, Graphene-wrapped hierarchical TiO_2 nanoflower composites with enhanced photocatalytic performance, J. Mater. Chem. A. 1 (2013) 12255–12262.

[55] N.R. Khalid, Z. Hong, E. Ahmed, Y. Zhang, H. Chan, M. Ahmad, Synergistic effects of Fe and graphene on photocatalytic activity enhancement of TiO_2 under visible light, Appl. Surf. Sci. 258 (2012) 5827–5834.

[56] L. Wan, Y. Gao, X. H. Xia, Q. R. Deng, G. Shao, Phase selection and visible light photo-catalytic activity of Fe-doped TiO_2 prepared by the hydrothermal method, Mater. Res. Bull. 46 (2011) 442–446.

[57] J. Zhu, F. Chen, J. Zhang, H. Chen, M. Anpo, Fe^{3+}-TiO_2 photocatalysts prepared by combining sol-gel method with hydrothermal treatment and their characterization, J. Photochem. Photobiol. A Chem. 180 (2006) 196–204.

[58] N. Farhangi, R. R. Chowdhury, Y. Medina-Gonzalez, M. B. Ray, P. A. Charpentier, Visible light active Fe doped TiO_2 nanowires grown on graphene using supercritical CO_2, Appl. Catal. B Environ. 110 (2011) 25–32.

Figure legends

Figure 1. FE-SEM image of GO sheets (a) and the amorphous TiO_2 with different Fe doping amounts (b).

Figure 2. X-ray diffraction patterns of amorphous TiO_2, anatase TiO_2 and G-TiO_2-Fe.

Figure 3. Raman spectra of bare amorphous TiO_2 NPs, anatase TiO_2, GO-amorphous TiO_2-Fe and G-TiO_2-Fe.

Figure 4. FE-SEM images of amorphous TiO_2 (a), anatase TiO_2 (b) and G-TiO_2-Fe (10) (c) and EDS analysis results (d, e) of G-TiO_2-Fe (10).

Figure 5. XPS core level spectra of Ti 2p (a), O 1s (b), C 1s (c), and Fe 2p (d) of G-TiO_2-Fe (10) sample.

Figure 6. Diffuse reflectance spectra (a) and plots of the Kubelka-Munk remission function (b) for TiO_2 NP, G-TiO_2-Fe (5), G-TiO_2-Fe (10) and G-TiO_2-Fe (20).

Figure 7. Photocatalytic degradation curves for anatase TiO_2, G-TiO_2-Fe (5), G-TiO_2-Fe (10) and G-TiO_2-Fe (20) under visible light (a) and solar light (b) as well as G-TiO_2-Fe (10) in dark condition.

Figure 8. Proposed mechanism for the enhanced visible light photocatalytic activity of G-TiO_2-Fe.

Figure 1

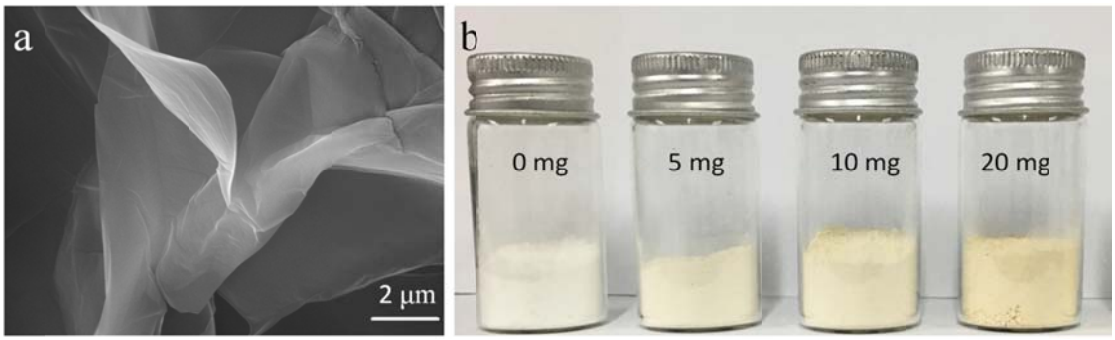

Figure 2

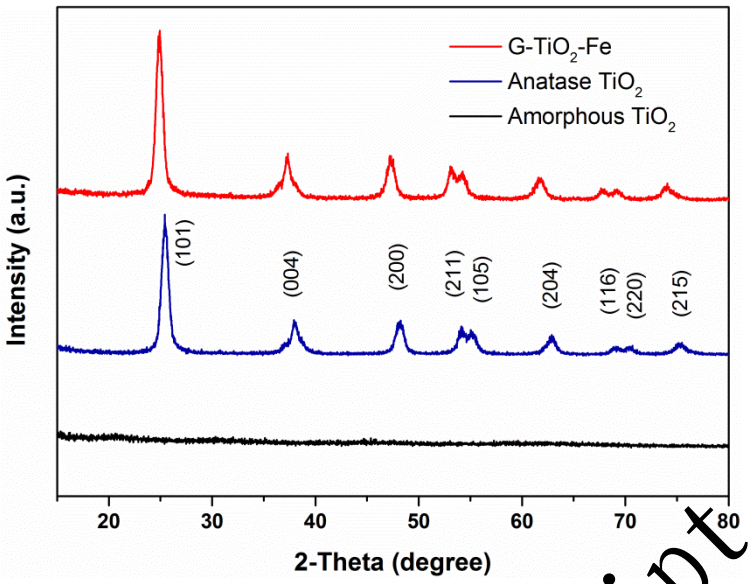

Figure 3

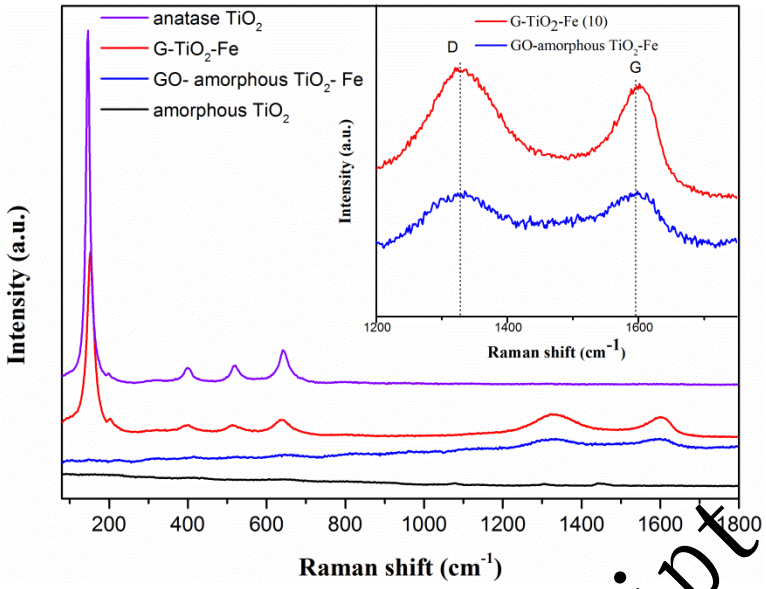

Figure 4

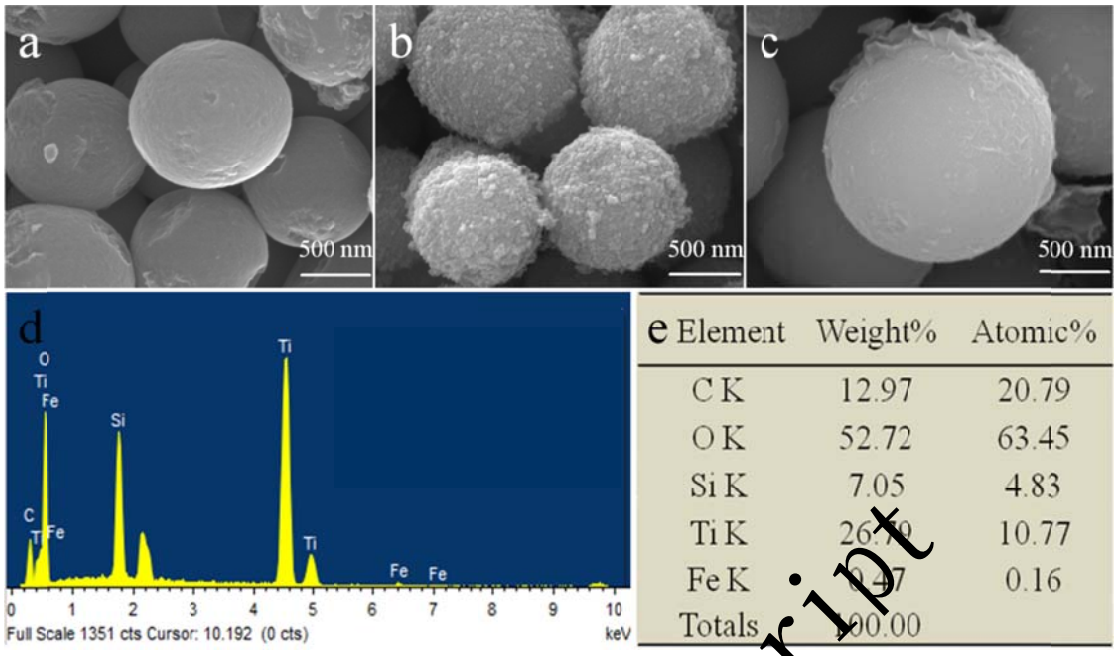

e

Element	Weight%	Atomic%
C K	12.97	20.79
O K	52.72	63.45
Si K	7.05	4.83
Ti K	26.79	10.77
Fe K	0.47	0.16
Totals	100.00	

Figure 5

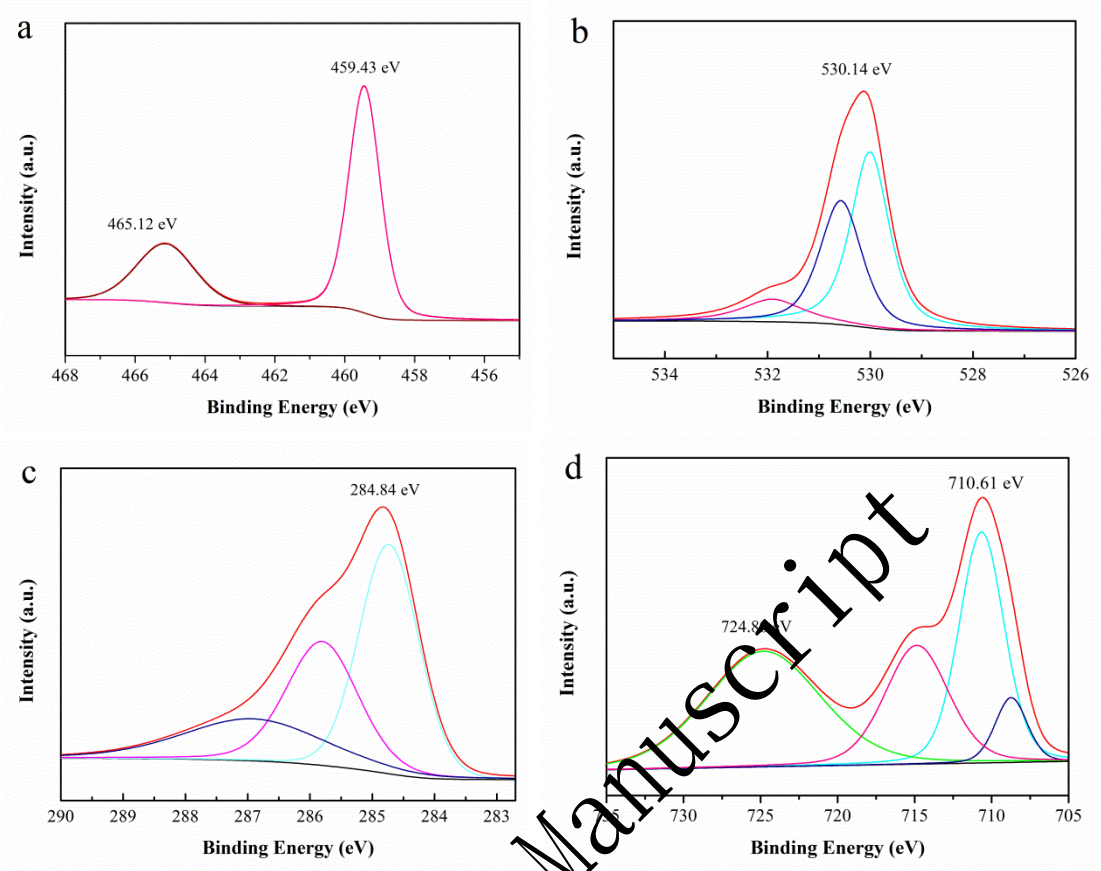

Figure 6

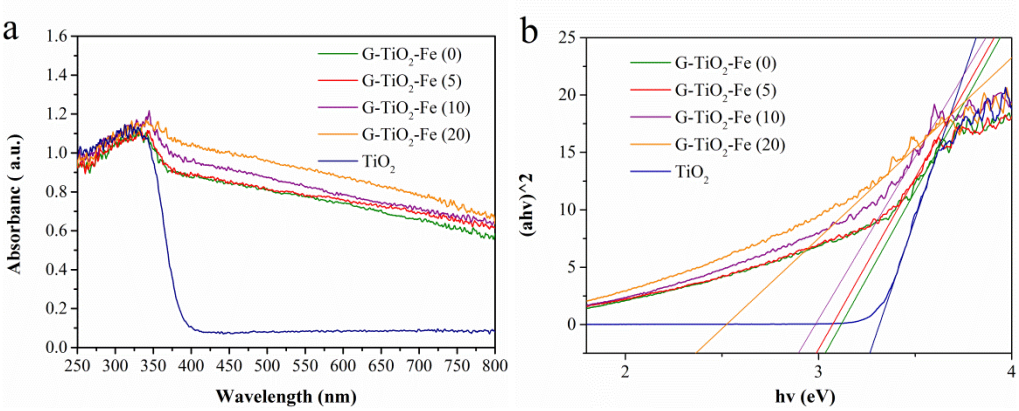

Figure 7

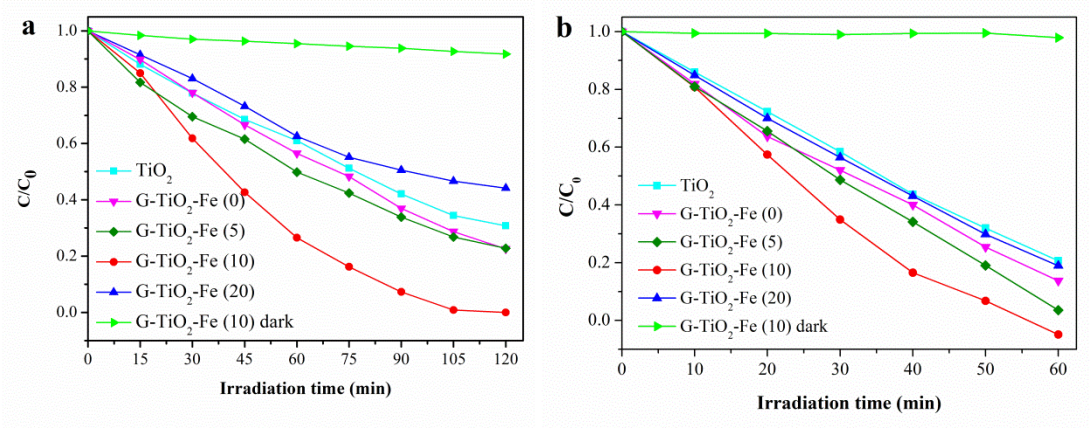

Figure 8